Canadian Mineralogist
Vol. 27, pp. 427-440 (1989)

HEMLOITE $(As,Sb)_2(Ti,V,Fe,Al)_{12}O_{23}OH$: A NEW MINERAL FROM THE HEMLO GOLD DEPOSIT, HEMLO, ONTARIO, AND ITS CRYSTAL STRUCTURE[1]

DONALD C. HARRIS
Geological Survey of Canada, 601 Booth Street, Ottawa, Ontario K1A 0E8

BERNARD F. HOSKINS AND IAN E. GREY
CSIRO Division of Mineral Products, P.O. Box 124, Port Melbourne, Victoria 3207, Australia

ALAN J. CRIDDLE AND CHRIS J. STANLEY
Department of Mineralogy, British Museum (Natural History), Cromwell Road, London, England SW7 5BD

ABSTRACT

Hemloite, ideally $(As,Sb)_2(Ti,V,Fe,Al)_{12}O_{23}OH$, is a rare constituent in drill core samples from the Hemlo gold deposit, Hemlo, Ontario. The mineral occurs as subhedral to anhedral grains up to 400 × 600 μm in size, associated with rutile, pyrite, molybdenite and arsenopyrite in a matrix of quartz, barian microcline and vanadian muscovite. Hemloite is black and opaque, with a submetallic to metallic luster and a black streak. No cleavage was observed; the fracture is curved to irregular. It is low to moderately reflecting, with a grey hue. Neither bireflectance nor pleochroism is detectable by eye. Between crossed polars, the mineral is very weakly anisotropic, with dark grey to dark brown rotation-tints. Measured reflectance values in air and oil are tabulated. Color values relative to the CIE C illuminant for R_1 and R_2 are: Y% 17.1, 17.8; λ_d 473, 474; and P_e % 2.6, 3.2. VHN_{100} 913 (range 858-967); calculated Mohs hardness is 6.5 to 7.0. X-ray studies show that the mineral is triclinic, space group $P\bar{1}$, with a 7.158(1), b 7.552(1), c 16.014(3) Å, α 89.06(1)°, β 104.32(2)°, γ 84.97(1)°, V 834.8(4) Å^3, a:b:c 0.9478:1:2.1205, Z = 2. D_{calc} = 4.613 g/cm^3. The structure has been determined and refined to R = 5.26% for 4850 unique reflections. There is a close structural relationship among hemloite, derbylite and tomichite. The hemloite structure comprises an ordered intergrowth, parallel to $(001)_n$, of tomichite-type structure and a new MX_2 structure-type that may be described as an ordered unit-cell intergrowth of rutile and goethite structure-types, parallel to $(001)_{rutile}$. The strongest six reflections of the X-ray powder pattern [d in Å(I)(hkl)] are: 3.045(70)(211,122), 2.924(100)(114), 2.799(80)($1\bar{2}2$), 2.722(90)($2\bar{1}\bar{4}$), 2.665(90)($22\bar{2}$) and 2.498(70)($11\bar{6}$). The name reflects the site of the deposit.

Keywords: hemloite, new mineral species, Hemlo gold deposit, Ontario, electron-microprobe analyses, reflectance data, X-ray powder data, crystal structure.

SOMMAIRE

La hemloïte, de composition idéale $(As,Sb)_2(Ti,V,Fe,Al)_{12}O_{23}OH$, est un rare composant de carottes de forage prélevées du gisement d'or de Hemlo, en Ontario. Les cristaux subidiomorphes à xénomorphes, qui atteignent 400 × 600 μm, sont associés à rutile, pyrite, molybdénite et arsenopyrite dans une gangue de quartz, microcline baryfère et muscovite vanadifère. La hemloïte est noir et opaque, avec un reflet submétallique ou métallique et une rayure noire. Elle est sans clivage; la surface des fractures est courbe ou irrégulière. Elle possède un reflet grisâtre faible ou modéré. Ni biréflectance, ni pléochroïsme n'a été décelé à l'oeil nu. C'est un minéral très faiblement anisotrope, avec les teintes de rotation de gris foncé à brun foncé. Nous présentons des valeurs de réflectance dans l'air et dans l'huile. Les valeurs de la couleur, comparées à celles de l'illuminant CIE C pour R_1 et R_2, sont: Y 17.1, 17.8%; λ_d 473, 474; P_e 2.6, 3.2. Les valeurs de VHN_{100} s'échelonnent entre 858 et 967 (moyenne 913); la dureté Mohs calculée est de 6.5 ou 7. Les études par diffraction X montrent qu'il s'agit d'un minéral triclinique, groupe spatial $P\bar{1}$, a 7.158(1), b 7.552(1), c 16.014(3) Å, α 89.06(1)°, β 104.32(2)°, γ 84.97(1)°, V 834.8(4) Å^3, a:b:c 0.9478:1:2.1205, Z = 2. D_{calc} = 4.613. La structure a été affinée jusqu'à un résidu R de 5.26% pour 4850 réflexions indépendantes. Les espèces hemloïte, derbylite et tomichite sont étroitement liées structuralement. La hemloïte contient une intercroissance ordonnée, parallèle à $(001)_n$, d'une structure semblable à celle de la tomichite et d'une nouvelle structure de stoechiométrie MX_2 que nous décrivons comme une intercroissance ordonnée, à l'échelle de la maille élémentaire, des structures du rutile et de la goethite, parallèles à (001) du rutile. Les six raies les plus intenses du cliché de poudre [d en Å(I)(hkl)] sont: 3.045(70)(211,122), 2.924(100)(114), 2.799(80)($1\bar{2}2$), 2.722(90)($2\bar{1}\bar{4}$), 2.665(90)($22\bar{2}$) et 2.498(70)($11\bar{6}$). Le nom rappelle le site du gisement.

(Traduit par la Rédaction)

Mots-clés: hemloïte, nouvelle espèce minérale, gisement d'or de Hemlo, Ontario, analyses à la microsonde électronique, données de réflectance, données de diffraction X (méthode des poudres), structure cristalline.

INTRODUCTION

Hemloite, ideally $(As,Sb)_2(Ti,V,Fe,Al)_{12}O_{23}OH$, is a newly described mineral species from the Hemlo gold deposit, Hemlo, Ontario. The mineral is named

---

[1] Geological Survey of Canada Contribution Number 25388.

after the site of the deposit. Hemlo, a former railroad station and a small settlement on the main transcontinental line of the Canadian Pacific railroad, is located three kilometers west of the mines. The mineral name and data have been approved by the Commission on New Minerals and Mineral Names, International Mineralogical Association. Type material is deposited at the British Museum (Natural History) as specimen BM 1986, 512, polished section E.1210, and as drill core and polished sections in the Systematic Reference Series of the National Mineral Collection, Geological Survey of Canada, Ottawa under catalogue number NMC 65544.

OCCURRENCE AND PHYSICAL PROPERTIES

The Hemlo gold deposit is located near the northeastern shore of Lake Superior, 35 km east of Marathon, adjacent to the Trans-Canada Highway 17, at latitude 48°40′N and longitude of 86°00′W. The deposit was discovered in 1982, and the combined total published gold reserves are approximately 80 million tonnes at 7.7 g/t Au. Three properties, covering portions of this single large deposit, have been brought into production within the last few years. They are, from east to west, the David Bell mine (formerly named the Teck–Corona mine), the Golden Giant mine and the Page–Williams mine. The gold deposit is enriched in Mo, Sb, As, Hg, Tl, V and Ba and contains a diverse assemblage of minerals. A comprehensive mineralogical study of the deposit was initiated in 1983, and some preliminary data on the mineralogy have been reported elsewhere (Harris 1986a, b).

Hemloite is a rare constituent within the deposit, having only been recognized in drill-core samples from hole W70, 742.6 and 746.8 m within the Page–Williams mine. This portion of the deposit also contains barian tomichite, which is physically similar to hemloite, but the two can be readily distinguished by their optical properties, chemical composition and X-ray powder-diffraction pattern. Grey *et al.* (1987) gave a description of barian tomichite from the deposit and also solved and refined its average structure, as well as that of tomichite. Hemloite and barian tomichite do not occur in the same polished sections. Hemloite occurs as subhedral to anhedral grains that attain 400 × 600 µm in size, in a quartz – barian microcline matrix. Some of these grains contain inclusions of pyrite and rare molybdenite, whereas in other grains, hemloite occurs as a rim on

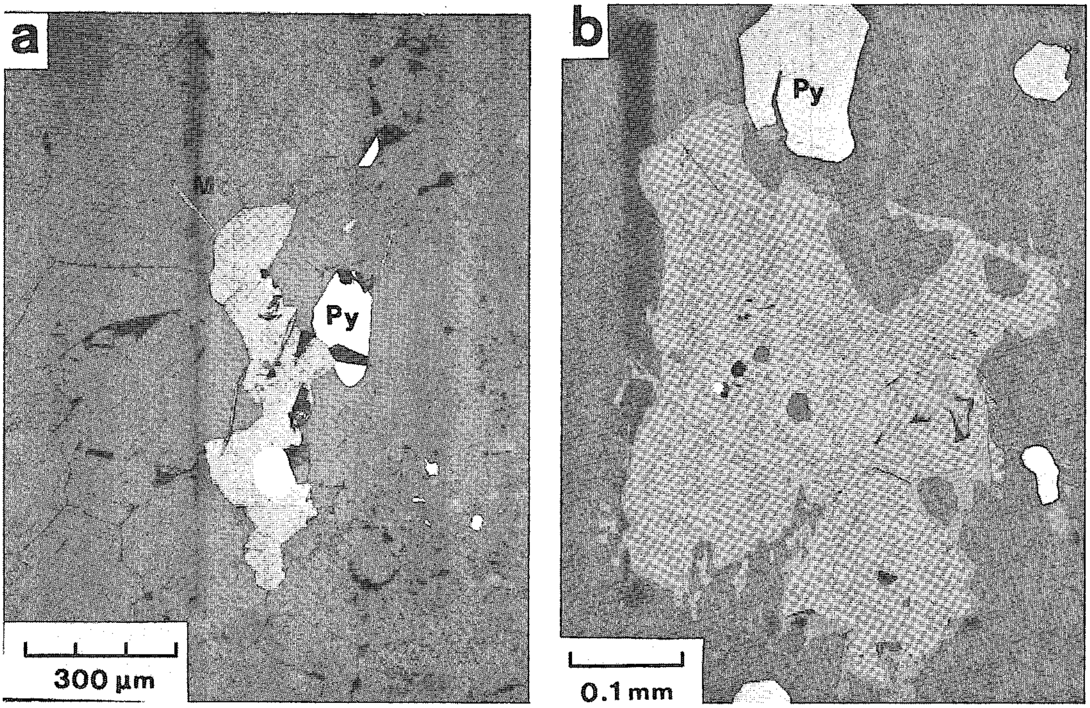

FIG. 1. a. Photomicrograph of an anhedral hemloite grain in quartz-microcline matrix associated with pyrite (white) and molybdenite. b. Coarse composite grain of hemloite surrounding rutile, with some alteration to titanite. The white grains are pyrite.

rutile and in turn is partially altered to titanite (Fig. 1). Other minerals observed in the hemloite-bearing polished sections are sphalerite, molybdenite, vanadian muscovite and rare arsenopyrite. Hemloite is opaque, with a metallic to submetallic luster and black with a black streak. Microhardness measurements, made with a Leitz Miniload 2 hardness tester on two grains, gave a VHN_{100} of 913 (mean of 10 indentations), with a range of 858–967. The indentations are perfect, with slight fracturing at their corners. The calculated Mohs hardness is in the range 6.5 to 7.0. No cleavage was observed; hemloite has a curved to irregular fracture. The density could not be measured because of the inclusions of pyrite and rutile, but the density calculated from the unit-cell contents is 4.613 g/cm³.

TABLE 1. ELECTRON MICROPROBE DATA ON HEMLOITE

Sample	As_2O_3	Sb_2O_3	TiO_2	V_2O_3	Fe_2O_3	Al_2O_3	Total
746.8-BM	12.5	5.8	38.1	13.4	26.7	1.4	97.9
746.8-1A	12.1	5.8	39.0	12.2	27.0	1.3	97.4
746.8-2A	12.0	5.7	39.0	12.7	27.0	1.3	97.7
746.8-3A	12.0	5.8	39.3	12.8	26.5	1.4	97.8
742.6	11.2	6.7	37.3	20.4	20.8	1.1	97.5

H_2O not determined. Values in wt.%

Formulae normalized to 46 oxygen atoms + 2 hydroxyl groups and 24 cations in the M site

746.8-BM	$(As_{2.98}Sb_{0.94}\square)(Ti_{11.25}V_{4.22}Fe^{2+}{}_{1.01}Fe^{3+}{}_{6.87}Al_{.65})O_{46}(OH)_2$
746.8-1A	$(As_{2.90}Sb_{0.94}\square)(Ti_{11.55}V_{3.85}Fe^{2+}{}_{1.06}Fe^{3+}{}_{6.94}Al_{.60})O_{46}(OH)_2$
746.8-2A	$(As_{2.85}Sb_{0.92}\square)(Ti_{11.47}V_{3.98}Fe^{2+}{}_{0.76}Fe^{3+}{}_{7.19}Al_{.60})O_{46}(OH)_2$
746.8-3A	$(As_{2.85}Sb_{0.93}\square)(Ti_{11.55}V_{4.01}Fe^{2+}{}_{0.81}Fe^{3+}{}_{6.98}Al_{.64})O_{46}(OH)_2$
742.6	$(As_{2.66}Sb_{1.08}\square)(Ti_{10.97}V_{6.40}Fe^{2+}{}_{0.18}Fe^{3+}{}_{5.94}Al_{.51})O_{46}(OH)_2$

BM = British Museum (Natural History). Instrument: Cambridge Instruments Microscan IX Accelerating voltage: 20 kV; beam current: 2.50×10-8 amps on Faraday cup.

Standards: TiO_2, Al_2O_3, FeS. V, As, Sb. Other samples: Geological Survey of Canada. Instrument: Cameca CAMEBAX
Accelerating voltage: 20 kV; beam current: 3.0×10-8 amps on Faraday cup
Standards: TiO_2, $FeAs_2$, Fe_3O_4, V_2O_5, Al_2O_3, synthetic $Cu_{11}FeSb_4S_{13}$.

CHEMICAL COMPOSITION

Results of electron-microprobe analyses are given in Table 1, together with the analytical procedures. Polished sections of drill core W70, 746.8 m contain most of the observed and analyzed grains of hemloite. Some of these were analyzed with a Cambridge Instruments Microscan IX at the British Museum (Natural History), and others were analyzed with a Cameca CAMEBAX at the Geological Survey of Canada. As shown in Table 1, grains within several polished sections of drill core 746.8 m are very consistent in composition, and only these samples were used for the full characterization of the mineral. The consistently low totals suggest the presence of H_2O or OH^-. However, the small grain-size and lack of material made it impossible to obtain direct measurements of H_2O content or of the valency states of Fe and V. Evidence for the presence of OH groups is provided by the crystal-structure data, which indicate two hydroxyl groups in each unit cell. By analogy with the related minerals derbylite and tomichite, the titanium is considered tetravalent, vanadium is trivalent, and a combination of ferrous and ferric iron is required for the charge balance. Microprobe analyses of rutile associated with some of the hemloite grains gave TiO_2 91.1, Sb_2O_3 3.8, V_2O_3 2.8, Fe_2O_3 0.6, WO_3 0.8, total 99.1 wt.%. The presence of Sb-V-W-bearing rutile in the Hemlo gold deposit is characteristic and is only observed within the ore zone.

TABLE 2. REFLECTANCE DATA FOR HEMLOITE

λnm	R_1	R_2	imR_1	imR_2
400	18.9	20.5	6.85	7.49
420	18.6	19.8	6.57	7.06
440	18.2	19.15	6.28	6.70
460	17.8	18.7	6.02	6.40
470	*17.7*	*18.5*	*5.91*	*6.27*
480	17.55	18.4	5.82	6.19
500	17.4	18.2	5.67	6.03
520	17.2	18.0	5.58	5.92
540	17.1	17.8	5.50	5.84
546	*17.1*	*17.8*	*5.48*	*5.82*
560	17.0	17.7	5.44	5.75
580	16.95	17.6	5.40	5.70
589	*16.9*	*17.5*	*5.38*	*5.67*
600	16.9	17.5	5.38	5.66
620	16.9	17.4	5.35	5.62
640	16.8	17.4	5.33	5.59
650	*16.8*	*17.35*	*5.31*	*5.59*
660	16.8	17.3	5.31	5.57
680	16.8	17.3	5.30	5.56
700	16.75	17.2	5.28	5.55

COLOR VALUES

C Illuminant				
x	.305	.305	.300	.299
y	.310	.309	.303	.302
Y%	17.1	17.8	5.5	5.8
λ_d	473	474	471	473
P_e%	2.6	3.2	5.5	6.0
A Illuminant				
x	.443	.442	.439	.438
y	.406	.405	.403	.402
Y%	17.0	17.7	5.4	5.8
λ_d	487	488	485	486
P_e%	1.1	1.4	2.3	2.6

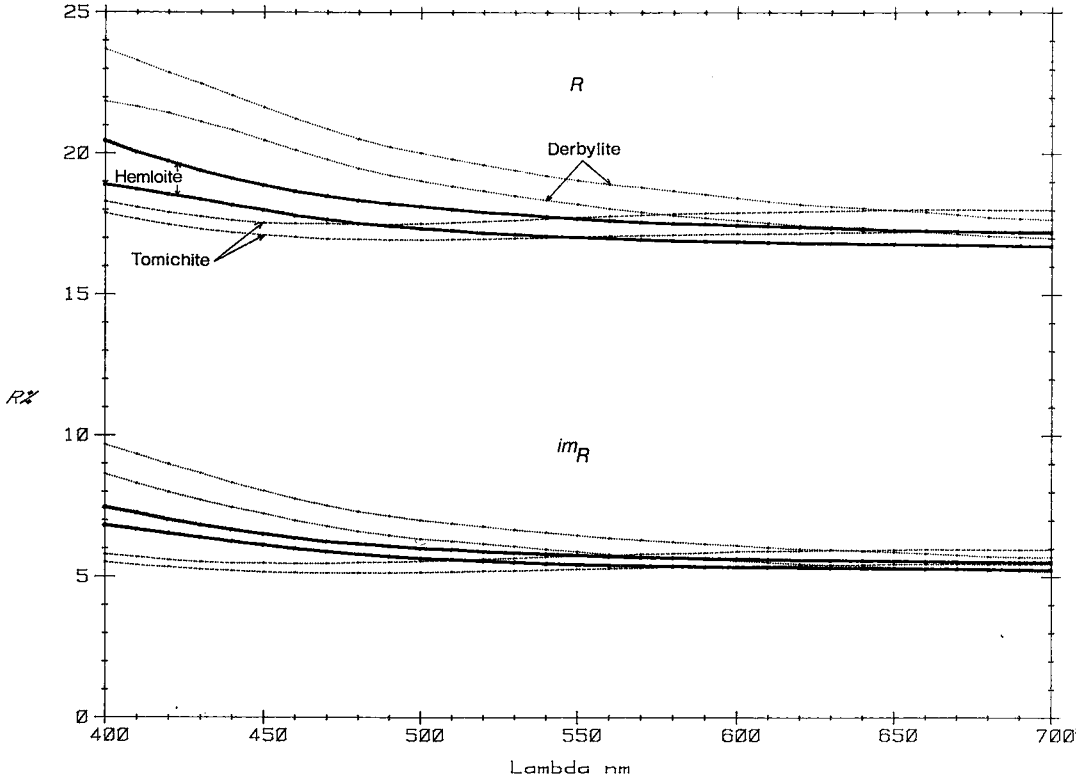

FIG. 2. Reflectance spectra R and ^{im}R between 400 and 700 nm for hemloite, tomichite and derbylite.

OPTICAL PROPERTIES

In plane-polarized reflected light (at about 3100 K), hemloite has a low to moderate reflectance, with a grey hue. Neither bireflectance nor pleochroism is detectable by eye, either in air or in oil. Between crossed polars, in both media, the mineral is very weakly anisotropic, with dark grey to dark brown rotation-tints. These tints are lightened, but not changed in hue, when the polarizers are uncrossed by 3°.

Reflectance measurements were made using the equipment and procedures described by Criddle *et al.* (1983). Silicon carbide (Zeiss, SiC no. 472) was used as a standard, and the effective numerical apertures of the × 16 air and oil (the latter used with Zeiss oil $N_D = 1.515$) were adjusted to 0.15.

In the absence of clearly defined positions of extinction (due to the very weak anisotropy of hemloite), the grains were oriented for measurement on the basis of the maximum and minimum readings from the photometer at 550 nm. Although hemloite is triclinic, these positions are orthogonal, which suggests straight extinction. The dispersion of the measured reflectance and bireflectance is weak, with a gentle monotonic reduction from 400 to 700 nm. R and ^{im}R data for the most bireflectant grain measured are shown in Table 2, together with color values. The color values were computed from the original data measured at an interval of 10 nm. For the C illuminant, the bireflectance is 0.7% absolute; the dominant wavelength is in the blue sector of the color chart; the excitation purity is low. Hemloite was first suspected to be a new mineral or, at least, a new variety, on the basis of differences between its reflectance spectra and those of type specimens of derbylite and tomichite. The optical properties of these minerals are described fully by Criddle *et al.* (in prep.), but differences in the reflectance spectra of the three minerals are summarized in Figure 2: derbylite has a higher reflectance than hemloite, significantly so at 400 nm, and it is marginally more bireflectant; the dispersion of tomichite is different from that of hemloite, with lower reflectance at 400 nm and higher reflectance at 700 nm. It is worth noting that since hemloite and tomichite have identical reflectances and bireflectance at 550 nm, their identification on the basis of reflectance measurements depends on the measurement of the dispersed reflectance for the full visible spectrum.

In general, the optical constants, indices of refraction n and absorption coefficients k may be derived from reflectance measurements at normal incidence in air and oil (Embrey & Criddle 1978). A limitation of this procedure is that it is impossible to determine the directions of principal vibration of absorbing triclinic minerals from their optical properties (Galopin & Henry 1972). Bearing this in mind, reflectance measurements on randomly oriented sections of triclinic minerals may be used to obtain an indication of the probable magnitude of the constants and of their dispersion. Through selection of the most bireflectant grains for measurement, the computed values for 'n and k' should approximate to the extreme values for the constants. In the case of hemloite, the values derived from the measured reflectance data (summarized in Table 2), using the Koenigsberger equations, indicate that the values for k_1 and k_2 decrease gradually from 0.65_1 and 0.55_2 at 400 nm, and converge slightly, to 0.36_1 and 0.34_2 at 700 nm (*i.e.*, $r<v$). The dispersion of n_2 follows a broadly similar and descending trend from 2.51 at 400 nm to 2.36 at 700 nm, whereas over the same range, n_1 increases marginally from 2.30 to 2.32. It is, of course, impossible to determine the sign of the birefringence from these measurements.

GLADSTONE–DALE RELATIONSHIP

The chemical molar refractivity (K_C) was calculated from the weight percentages of the constituents for sample 746.8–BM (Table 1) using the revised Gladstone–Dale constants of Mandarino (1981), and assuming water by difference. The density of the mineral was not measurable; hence, in the calculation of K_P, the value of the density calculated from the unit-cell contents had been adjusted to allow for the water content.

Hemloite is demonstrably absorbing; hence it follows that if the absorption is overlooked, the refringences derived from the reflectances are likely to be too low, and this should be reflected in the test for compatibility, $1-(K_P/K_C)$, recommended by Mandarino (1979). A further problem has already been high-lighted; though the mineral is triclinic, only the probable values for the most extreme refringences could be obtained from the reflectance data. In taking the mean ($2.35_{590\text{nm}}$) of these values (2.32 and 2.38), it is possible that a bias has been introduced (*i.e.*, the index of refraction for β may be closer to either α or γ). Neglecting the absorption, the compatibility index for sample 746.8–BM is 0.065 (fair) and for the ideal composition, 0.052 (good). Including the absorption coefficient, and using the modulus of the complex index, ($\sqrt{n^2+k^2}$), the compatibility index for sample 746.8–BM is 'improved' to 0.038 (excellent), as it is for the ideal composition, 0.024 (excellent). Encouraging as these results appear, it is stressed that K_C was calculated assuming water by difference. The structural interpretation supports this assumption, but direct evidence is lacking.

TABLE 3. X-RAY POWDER DATA FOR HEMLOITE

Iest.	d Å (meas.)	d calc.	hkl
5	4.928	4.930	$1\bar{1}\bar{1}$
10	4.058	4.066	$11\bar{3}$
5	3.818	3.810	$10\bar{4}$
20	3.212	3.231 3.207	$1\bar{1}3$ $1\bar{2}\bar{1}$
40	3.121	3.115	$2\bar{1}\bar{1}$
70	3.045	3.055 3.047	211 122
100	2.924	2.917	114
80	2.799	2.798	$1\bar{2}2$
90	2.722	2.717	$2\bar{1}\bar{4}$
90	2.665	2.665	$22\bar{2}$
70	2.498	2.493	$11\bar{6}$
10	2.455	2.458 2.440	$03\bar{1}$ 025
20	2.406	2.406	222
40	2.280	2.281	$21\bar{6}$
50	2.217	2.225 2.208 2.141	$1\bar{3}1$ 125 $23\bar{1}$
50	2.135	2.133	$2\bar{2}\bar{5}$
5	2.110	2.112	116
40	2.069	2.071	$1\bar{2}5$
5	2.029	2.030	$2\bar{1}\bar{7}$
50	1.971	1.971	107
5	1.940	1.942	$31\bar{6}$
5	1.898	1.895	$32\bar{5}$
5	1.875	1.876	225
10	1.800	1.804 1.800	$33\bar{1}$ $3\bar{2}\bar{5}$
60	1.774	1.776 1.771	$1\bar{2}\bar{8}$ $2\bar{1}6$
10	1.726	1.720	240
20	1.695	1.694	$14\bar{4}$
5	1.677	1.676	332
60	1.621	1.621	$41\bar{6}$
60B	1.579	1.591 1.579 1.571	243 $3\bar{3}1$ 325
5	1.554	1.550	00.10
5	1.528	1.528	340
60	1.508	1.510 1.508 1.504	$43\bar{1}$ $4\bar{2}\bar{5}$ $03\bar{8}$
5	1.484	1.482	$3\bar{1}6$
5	1.467	1.467	$30.\overline{10}$
40	1.446	1.444	$14\bar{7}$
50	1.434	1.437	$1\bar{1}.\overline{11}$
40	1.420	1.435	$33\bar{8}$
5	1.399		
40	1.373		
40	1.358		
5	1.332		
5	1.250		
5	1.210		

Triclinic, $P\bar{1}$ a 7.158(1), b 7.552(1), c 16.014(3)Å, σ89.06(1), β104.32(2), γ84.97(1)°

114.6 mm Debye-Scherrer camera. Cu radiation, Ni filter CuKα 1.54178Å). Indices assigned from the calculated X-ray powder diffraction pattern based on atomic coordinates obtained from the single crystal studies.

X-RAY STUDIES (POWDER DATA)

The X-ray powder-diffraction data for hemloite are listed in Table 3. Owing to the presence of Fe, Ti and V, some fluorescence was obtained with Cu radiation, but Mo radiation was found to be unsuitable because of the excessive contraction of the pattern. Film-shrinkage corrections could not be applied owing to the absence of back reflections. The unit-cell parameters were obtained from the results of the single-crystal structure refinement; the indices are based on the calculated pattern using the atomic coordinates, for which the refinement converged with $R=5.26\%$.

TABLE 4. CRYSTAL DATA FOR HEMLOITE

Hemloite	$As_{1.49}Sb_{0.47}Ti_{5.63}V_{2.11}Fe_{3.94}Al_{0.32}O_{23}OH$
Formula Weight	1159.7
Crystal System	triclinic, $P\bar{1}$

	reference cell		reduced cell	
a, Å	7.158	(1)	7.552	(1)
b, Å	7.552	(1)	15.842	(2)
c, Å	16.014	(3)	7.158	(1)
α, deg.	89.06	(1)	78.36	(1)
β, deg.	104.32	(2)	84.97	(1)
γ, deg.	84.97	(1)	86.78	(2)
V, Å^3	834.8	(4)		
a:b:c	0.9478:1:2.1205		0.4767:1:0.4518	
Z	2			

Density: D_{calc} (g/cm^3)	4.613; D_{obs} not measured	
Linear absorption coefficient:	μ (Mo Kα)	106.9 cm^{-1}
Crystal dimensions	±(33$\bar{5}$)	0.043
(distance in mm from centroid)	±(001)	0.115
	±(111)	0.072
radiation	Mo Kα (graphite monochromator) λ = 0.71069Å	
transmission factors	max 0.444	min 0.180
F(000)	1090	
2θ limits	$2° < 2\theta < 60°$ ($-5 < h < 10$, $-10 < k < 10$, $-22 < \ell < 22$)	
no. of reflections collected	8445	
no. of unique reflections	4850	
Ramal	1.69%	
no. of unique reflection used	($I > 3\sigma(I)$)	3547
Final R	5.26%	
Final Rw	5.60%	

SINGLE-CRYSTAL STUDIES

A preliminary study of individual grains using the precession method showed them to be untwinned triclinic single crystals. Certain reciprocal-lattice sections were observed to be similar to those obtained from barian tomichite (Grey *et al.* 1987), indicating a structural relationship between the two minerals. The diffuse diffraction-maxima produced by barian tomichite were not observed in the precession photographs of hemloite.

For collection of the intensity data, a crystal fragment was mounted about an arbitrary direction on an Enraf–Nonius CAD4F diffractometer. Accurate values of the unit-cell parameters and crystal-orientation matrix were determined from a least-squares treatment of the angular settings of 25 centered reflections with $11 < \theta < 18°$ for Mo*Kα* radiation. Details of the data collection are given in Table 4. Intensity measurements were made with the ω–2θ mode. Three strong reflections were used as orientation controls (every 100 reflections) as well as intensity monitors (every 3000 seconds of X-ray exposure time). There was no significant variation in intensity values of the control reflections during the data collection. Corrections for Lorentz, polarization and absorption effects were applied. Absorption corrections were numerically evaluated by Gaussian integration to a precision of 0.5% (Sheldrick 1976).

SOLUTION AND REFINEMENT OF THE STRUCTURE

The structure of hemloite was solved in space group $P\bar{1}$ using a combination of direct and Fourier methods. The interpretation of the E-maps was facilitated by making use of the structural relationship with barian tomichite observed on precession photographs. To take advantage of this relationship, it was necessary to transform the reduced cell so that two axes lie in a plane parallel to the layers of closest-packed anions that are common to the two structures. The transformation matrix from the reduced to the working cell is 100/010/$\bar{1}$01; both unit cells are given in Table 4.

The metal atoms were all located in an E-map generated with the program MULTAN (Main *et al.* 1977). Fourier maps revealed the location of all oxygen atoms and also showed a disorder in the distribution of the arsenic atom. The disorder required fractional occupancy of two sites separated by 2.4 Å.

The structure was refined by using the full-matrix least-squares facility of the SHELX–76 system (Sheldrick 1976), which minimizes the function $\Sigma w\Delta^2$, where $\Delta = |F_o| - |F_c|$ and w is the weight assigned to each reflection. A weighting scheme of the form $w = [k/\sigma^2(F) + 0.001\,|F|^2]$ was applied, where k was redetermined after each cycle of refinement. An analysis of variance at the end of the refinement showed no unusual features, indicating that the weighting scheme used was appropriate.

Considerable care was taken to establish the distribution of arsenic and antimony among the three crystallographically independent sites A(1)–A(3). Unconstrained refinement of individual site-occupancy factors (*SOF*) for arsenic and antimony on each site showed that antimony is ordered only in site A(1), with almost full occupancy of A(1) by As + Sb. The remaining two sites are partially occupied by arsenic only, with the sum of the *SOF*s for the two sites being close to unity. In subsequent refinements the antimony content from the chemical analysis was assigned to site A(1) and kept fixed. The arsenic *SOF*s of the three sites were refined. The calculated unit-cell content of arsenic derived from the refinement is 2.95 atoms, in reasonable agreement with the value of 2.98 atoms from the microprobe analysis.

The twelve independent metal atom sites, *M*(1)–*M*(12), are occupied by 5.63Ti + 2.11V + 3.94Fe + 0.32Al (from chemical analyses). Unambiguous site-assignments of these atoms could not be definitely established from the refinement because of the similarity in their scattering-factor values. The scattering curve for vanadium was used at the twelve sites since it approximates closely the composite scattering-curve for the above combination of elements. Scattering curves for neutral atoms, together with corrections for anomalous dispersion, were taken from the International Tables for X-ray Crystallography (1974). The final refinement, with anisotropic thermal parameters, involved 355 independent parameters, and the largest error was 0.1%. Final R-factors are given in Table 4. The largest feature in the final difference Fourier map is a peak of height ~2e/Å^3, 0.89 Å from A(1).

The distribution of arsenic and antimony atoms was also investigated in the corresponding noncentrosymmetric space-group $P1$. No significant difference was found from that obtained for the $P\bar{1}$ model, and there was no measurable improvement in the refinement.

Final atomic positions and thermal parameters are given in Table 5. Selected bond-lengths and angles are given in Table 6. Table 7, listing the observed and calculated structure-factors, is available from the Depository of Unpublished Data, CISTI, National Research Council of Canada, Ottawa, Ontario K1A 0S2.

DESCRIPTION OF STRUCTURE

A polyhedral representation of the structure of hemloite, viewed along a^* (Fig. 3) shows the essential close-packed nature of the structure, with closest-packed layers of anions parallel to (100). The stacking sequence along a^* of the anion layers is ABABCBCACA, *i.e.*, (*hhc*--), the same as for derbylite (Moore & Araki 1976) and barian tomichite (Grey *et al.* 1987). Indeed, there is a close structural relationship between hemloite and these minerals. The unit-cell transformation is given by $a_h = a_t$, $b_h = ½ (b_t - c_t)$, $c_h = 1/5 (2b_t + 15c_t)$, where the subscripts h and t refer to hemloite and tomichite, respectively.

The hemloite structure comprises an ordered intergrowth, parallel to $(001)_h$, of tomichite-type structure and a new MX_2 structure-type, which is illustrated in Figure 4. The latter may be described as an ordered unit-cell intergrowth of rutile and goethite structure-types, parallel to $(100)_{rutile}$. Disordered intergrowths of these two structure-types have previously been proposed to explain the complex diffraction patterns of the γ-MnO$_2$ series of phases (de Wolff 1959).

The relationship between the metal-atom distributions for equivalent layers in the hemloite and tomichite structures is shown in Figure 5. In tomichite, as in derbylite, the metal atoms lying

TABLE 5. HEMLOITE: ATOMIC COORDINATES AND THERMAL PARAMETERS (Å^2)*

Atom**	X	Y	Z	U_{11}	U_{22}	U_{33}	U_{23}	U_{13}	U_{12}
A(1)	0.58105(9)	0.27632(8)	-0.36243(4)	0.0071(3)	0.0083(3)	0.0240(3)	-0.0085(2)	-0.0007(2)	-0.0006(2)
A(2)	0.5846(1)	0.0580(1)	-0.0724(1)	0.0070(5)	0.0074(4)	0.0206(5)	-0.0061(3)	0.0007(4)	-0.0010(3)
A(3)	0.4135(3)	0.1690(3)	-0.2158(1)	0.0073(10)	0.0062(9)	0.0093(9)	-0.0014(7)	0.0048(7)	-0.0030(7)
M(1)	0.0005(1)	-0.2132(1)	-0.0353(1)	0.0041(5)	0.0036(4)	0.0039(4)	0.0003(3)	0.0017(3)	-0.0014(3)
M(2)	-0.0018(2)	0.1142(1)	-0.1473(1)	0.0117(6)	0.0089(5)	0.0108(5)	-0.0008(4)	0.0049(4)	-0.0021(4)
M(3)	0.0016(1)	0.0142(1)	-0.3316(1)	0.0056(5)	0.0044(4)	0.0049(4)	0.0001(3)	0.0031(4)	-0.0013(3)
M(4)	0.0057(1)	0.4401(1)	-0.2593(1)	0.0045(5)	0.0032(4)	0.0037(4)	0.0004(3)	0.0026(4)	-0.0013(3)
M(5)	0.0039(2)	0.3396(1)	-0.4484(1)	0.0076(5)	0.0060(5)	0.0078(5)	0.0006(4)	0.0046(4)	-0.0022(4)
M(6)	0.3139(2)	0.4198(1)	-0.0541(1)	0.0074(5)	0.0058(5)	0.0074(5)	-0.0009(4)	0.0036(4)	-0.0029(4)
M(7)	0.3154(2)	0.7520(1)	-0.1648(1)	0.0072(5)	0.0054(5)	0.0063(5)	0.0000(4)	0.0036(4)	-0.0010(4)
M(8)	0.3143(2)	0.6489(1)	-0.3497(1)	0.0084(5)	0.0065(4)	0.0082(5)	-0.0008(4)	0.0040(4)	-0.0025(4)
M(9)	0.3115(1)	0.9729(1)	-0.4638(1)	0.0035(5)	0.0014(4)	0.0040(4)	0.0003(3)	0.0029(4)	-0.0006(3)
M(10)	0.6852(2)	0.4771(1)	-0.1298(1)	0.0083(5)	0.0061(5)	0.0072(5)	0.0001(4)	0.0038(4)	-0.0006(4)
M(11)	0.6847(2)	0.8123(1)	-0.2388(1)	0.0075(5)	0.0058(5)	0.0066(5)	0.0000(4)	0.0031(4)	-0.0029(4)
M(12)	0.6894(2)	0.7027(1)	-0.4163(1)	0.0077(5)	0.0055(4)	0.0060(4)	0.0000(3)	0.0046(4)	-0.0006(4)
O(1)	-0.1589(7)	-0.2357(6)	0.0522(3)	0.011(2)	0.007(2)	0.012(2)	-0.002(2)	0.005(2)	-0.002(2)
O(2)	-0.1514(7)	0.0499(6)	-0.0648(3)	0.011(2)	0.010(2)	0.015(2)	-0.002(2)	0.008(2)	-0.003(2)
O(3)	-0.1797(6)	-0.3089(5)	-0.1292(3)	0.010(2)	0.006(2)	0.010(2)	-0.000(2)	0.004(2)	-0.002(2)
O(4)	0.1785(7)	-0.4183(6)	0.0105(3)	0.010(2)	0.009(2)	0.007(2)	-0.002(2)	0.001(2)	-0.001(2)
O(5)	0.1595(7)	-0.1113(6)	-0.1089(3)	0.015(2)	0.007(2)	0.012(2)	-0.003(2)	0.005(2)	-0.001(2)
O(6)	-0.1625(7)	0.3407(6)	-0.1871(3)	0.013(2)	0.006(2)	0.012(2)	-0.001(2)	0.003(2)	-0.001(2)
O(7)	-0.1573(7)	-0.0056(6)	-0.2440(3)	0.012(2)	0.006(2)	0.012(2)	-0.002(2)	0.005(2)	-0.001(2)
O(8)	0.1459(7)	0.1779(6)	-0.2320(3)	0.013(2)	0.007(2)	0.012(2)	-0.002(2)	0.008(2)	-0.003(2)
O(9)	-0.1543(7)	0.2781(6)	-0.3620(3)	0.009(2)	0.012(2)	0.008(2)	0.000(2)	0.006(2)	-0.001(2)
O(10)	-0.1816(6)	-0.0776(5)	-0.4207(3)	0.009(2)	0.006(2)	0.010(2)	0.000(2)	0.004(2)	-0.003(2)
O(11)	0.1813(6)	-0.1851(6)	-0.2850(3)	0.008(2)	0.007(2)	0.008(2)	0.001(2)	0.004(2)	0.001(2)
O(12)	0.1501(7)	0.1167(6)	-0.4058(3)	0.012(2)	0.006(2)	0.010(2)	-0.001(2)	0.005(2)	-0.003(2)
O(13)	-0.1695(7)	0.6474(6)	-0.2994(3)	0.011(2)	0.009(2)	0.008(2)	-0.001(2)	0.003(2)	-0.002(2)
O(14)	0.1821(7)	0.5366(5)	-0.1630(3)	0.011(2)	0.005(2)	0.010(2)	-0.000(2)	0.003(2)	-0.003(2)
O(15)	0.1631(7)	0.4634(6)	-0.3456(3)	0.014(2)	0.008(2)	0.006(2)	-0.003(2)	0.006(2)	-0.004(2)
O(16)	-0.1543(7)	0.5757(6)	-0.4770(3)	0.011(2)	0.007(2)	0.012(2)	-0.003(2)	0.008(2)	-0.002(2)
O(17)	-0.1787(6)	0.2409(6)	-0.5421(3)	0.009(2)	0.008(2)	0.008(2)	-0.001(2)	0.002 2)	-0.002(2)
O(18)	0.5007(6)	0.6207(6)	-0.0622(3)	0.009(2)	0.008(2)	0.007(2)	0.000(2)	0.003(2)	0.000(2)
O(19)	0.5016(7)	0.2841(6)	-0.1172(3)	0.011(2)	0.009(2)	0.017(2)	-0.003(2)	0.007(2)	-0.001(2)
O(20)	0.5035(7)	0.9437(6)	-0.1735(3)	0.011(2)	0.011(2)	0.013(2)	-0.003(2)	0.004(2)	-0.002(2)
O(21)	0.4999(6)	0.6100(6)	-0.2294(3)	0.008(2)	0.007(2)	0.011(2)	-0.001(2)	0.005(2)	-0.002(2)
O(22)	0.5021(6)	0.8478(5)	-0.3560(3)	0.010(2)	0.006(2)	0.008(2)	0.002(2)	0.005(2)	0.001(2)
O(23)	0.5126(7)	0.5144(6)	-0.4013(3)	0.011(2)	0.006(2)	0.013(2)	0.001(2)	0.004(2)	-0.005(2)
O(24)	0.5031(7)	0.8239(6)	-0.5260(3)	0.009(2)	0.007(2)	0.011(2)	-0.004(2)	0.002(2)	-0.000(2)

* Estimated standard deviations given in parentheses. Temperature factor = $\exp [-2\pi^2(h^2a^{*2}U_{11} + \ldots + 2hka^*b^*U_{12})]$.

** Site occupancies for A sites: A(1) 0.47Sb, 0.474(2)As; A(2) 0.685(2)As; A(3) 0.315(2)As.

TABLE 6. INTERATOMIC DISTANCES (Å) AND ANGLES (°) IN HEMLOITE*

M(1) Octahedron

			distance	angle
M(1)-O(1)	2.028(5)	O(1)-O(2)	2.847(7)	85.4(2)
M(1)-O(2)	2.166(4)	O(1)-O(2)a	2.698(7)	80.0(2)
M(1)-O(2)a	2.168(5)	O(1)-O(3)	2.937(7)	96.1(2)
M(1)-O(3)	1.920(5)	O(1)-O(4)	2.902(7)	94.4(2)
M(1)-O(4)	1.927(5)	O(5)-O(2)	2.695(7)	80.2(2)
M(1)-O(5)	2.016(6)	O(5)-O(2)a	2.841(7)	85.2(2)
Mean	2.038	O(5)-O(3)	2.914(7)	95.5(2)
		O(5)-O(4)	2.953(7)	96.9(2)
		O(2)-O(2)a	2.648(8)	75.3(2)
		O(2)-O(3)	2.921(6)	91.1(2)
		O(4)-O(2)a	2.933(6)	91.3(2)
		O(4)-O(3)	2.999(6)	102.4(2)
		Mean	2.857	89.5

M(2) Octahedron

			distance	angle
M(2)-O(1)a	1.962(5)	O(1)a-O(2)	2.698(7)	86.5(2)
M(2)-O(2)	1.974(6)	O(1)a-O(5)	2.787(7)	90.3(2)
M(2)-O(5)	1.970(4)	O(1)a-O(6)	2.785(6)	90.0(2)
M(2)-O(6)	1.978(4)	O(1)a-O(8)	2.899(7)	94.3(2)
M(2)-O(7)	1.956(5)	O(7) -O(2)	2.897(7)	95.0(2)
M(2)-O(8)	1.992(6)	O(7) -O(5)	2.768(6)	89.7(2)
Mean	1.972	O(7) -O(6)	2.784(6)	90.1(2)
		O(7) -O(8)	2.645(7)	84.2(2)
		O(5) -O(2)	2.695(7)	86.2(2)
		O(5) -O(8)	2.897(7)	94.0(2)
		O(6) -O(2)	2.901(7)	94.4(2)
		O(6) -O(8)	2.691(7)	85.4(2)
		Mean	2.787	90.0

M(3) Octahedron

			distance	angle
M(3)- O(7)	2.024(6)	O(7)- O(8)	2.645(7)	78.6(2)
M(3)- O(8)	2.148(5)	O(7)- O(9)	2.838(7)	84.8(2)
M(3)- O(9)	2.183(4)	O(7)-O(10)	2.856(7)	94.2(2)
M(3)-O(10)	1.871(5)	O(7)-O(11)	2.889(7)	94.8(2)
M(3)-O(11)	1.900(4)	O(12)- O(8)	2.836(7)	87.0(2)
M(3)-O(12)	1.970(6)	O(12)- O(9)	2.654(7)	79.3(2)
Mean	2.016	O(12)-O(10)	2.862(7)	96.3(2)
		O(12)-O(11)	2.923(7)	98.1(2)
		O(10)-O(11)	2.980(6)	104.4(2)
		O(10)- O(9)	2.867(6)	89.7(2)
		O(8)-O(11)	2.891(6)	90.9(2)
		O(8)- O(9)	2.641(6)	75.2(2)
		Mean	2.823	89.4

M(4) Octahedron

			distance	angle
M(4)- O(6)	2.042(6)	O(6)- O(8)	2.691(7)	80.4(2)
M(4)- O(8)	2.127(4)	O(6)- O(9)	2.862(7)	84.5(2)
M(4)- O(9)	2.212(5)	O(6)-O(13)	2.898(7)	94.2(2)
M(4)-O(13)	1.913(4)	O(6)-O(14)	2.934(7)	95.1(2)
M(4)-O(14)	1.934(5)	O(15)- O(8)	2.829(7)	86.4(2)
M(4)-O(15)	2.002(6)	O(15)- O(9)	2.732(7)	80.7(2)
Mean	2.038	O(15)-O(13)	2.911(7)	96.0(2)
		O(15)-O(14)	2.957(7)	97.4(2)
		O(13)-O(14)	2.942(6)	99.8(2)
		O(13)- O(9)	2.981(6)	92.3(2)
		O(8)-O(14)	2.951(6)	93.1(2)
		O(8)- O(9)	2.641(6)	75.0(2)
		Mean	2.861	89.6

M(5) Octahedron

			distance	angle
M(5)- O(9)	2.064(6)	O(9) -O(12)	2.654(2)	83.4(2)
M(5)-O(12)	1.922(4)	O(9) -O(15)	2.732(7)	83.3(2)
M(5)-O(15)	2.047(5)	O(9) -O(16)	2.882(7)	90.1(2)
M(5)-O(16)	2.008(4)	O(9) -O(17)	2.866(7)	91.5(2)
M(5)-O(16)b	1.931(6)	O(16)b-O(12)	2.969(7)	100.8(2)
M(5)-O(17)	1.937(5)	O(16)b-O(15)	2.847(7)	91.3(2)
Mean	1.985	O(16)b-O(16)	2.668(9)	85.3(2)
		O(16)b-O(17)	2.815(7)	93.4(2)
		O(12) -O(15)	2.806(6)	89.9(2)
		O(12) -O(17)	2.861(6)	95.7(2)
		O(16) -O(15)	2.747(6)	85.2(2)
		O(16) -O(17)	2.754(6)	88.5(2)
		Mean	2.800	89.9

M(6) Octahedron

			distance	angle
M(6)- O(1)a	1.858(5)	O(1)a- O(4)c	2.817(7)	95.1(2)
M(6)- O(4)c	1.958(5)	O(1)a-O(14)	2.902(7)	100.2(2)
M(6)-O(14)	1.923(5)	O(1)a-O(18)d	2.965(6)	100.3(2)
M(6)-O(18)	2.131(5)	O(1)a-O(19)	2.940(8)	96.3(2)
M(6)-O(18)d	2.003(4)	O(18) - O(4)c	2.588(6)	81.6(2)
M(6)-O(19)	2.083(5)	O(18) -O(14)	2.584(6)	79.0(2)
Mean	1.993	O(18) -O(18)d	2.681(9)	80.8(2)
		O(18) -O(19)	2.704(6)	79.8(2)
		O(14) - O(4)c	2.811(7)	92.8
		O(14) -O(19)	2.786(6)	88.0
		O(18)d- O(4)c	2.588(6)	81.6
		O(18)d-O(18)	2.681(9)	80.8
		Mean	2.754	88.0

M(7) Octahedron

			distance	angle
M(7)- O(5)c	1.853(5)	O(5)c-O(11)c	2.921(7)	100.0(2)
M(7)-O(11)c	1.958(5)	O(5)c-O(14)	2.814(6)	95.1(2)
M(7)-O(14)	1.960(5)	O(5)c-O(18)	2.967(6)	99.9(2)
M(7)-O(18)	2.020(4)	O(5)c-O(20)	2.955(8)	97.0(2)
M(7)-O(20)	2.087(5)	O(21) -O(11)c	2.598(6)	79.4(2)
M(7)-O(21)	2.104(5)	O(21) -O(14)	2.830(8)	88.2(2)
Mean	1.997	O(21) -O(18)	2.679(7)	81.0(2)
		O(21) -O(20)	2.688(6)	79.8(2)
		O(11)c-O(14)	2.843(7)	93.0(2)
		O(11)c-O(20)	2.810(6)	87.9(2)
		O(18) -O(14)	2.584(2)	81.0(2)
		O(18) -O(20)	3.002(7)	93.9(2)
		Mean	2.808	89.7

M(8) Octahedron

			distance	angle
M(8)-O(11)c	1.972(5)	O(11)c-O(15)	2.844(6)	96.0(2)
M(8)-O(15)	1.854(5)	O(11)c-O(17)b	2.805(7)	92.8(2)
M(8)-O(17)b	1.902(4)	O(11)c-O(21)	2.598(6)	80.4(2)
M(8)-O(21)	2.052(4)	O(11)c-O(22)	2.837(8)	87.7(2)
M(8)-O(22)	2.119(5)	O(23) -O(15)	2.909(8)	97.2(2)
M(8)-O(23)	2.021(5)	O(23) -O(17)b	2.837(6)	92.6(2)
Mean	1.987	O(23) -O(21)	2.878(7)	89.9(2)
		O(23) -O(22)	2.632(6)	78.9(2)
		O(15) -O(17)b	2.871(7)	99.7(2)
		O(15) -O(21)	2.969(6)	98.9(2)
		O(22) -O(17)b	2.629(6)	81.5(2)
		O(22) -O(21)	2.690(7)	80.3(2)
		Mean	2.792	89.7

M(9) Octahedron

			distance	angle
M(9)-O(10)b	1.971(5)	O(10)b-O(12)c	2.845(7)	94.4(2)
M(9)-O(12)c	1.929(5)	O(10)b-O(17)b	3.073(6)	103.0(2)
M(9)-O(17)b	1.957(5)	O(10)b-O(24)	2.810(6)	86.1(2)
M(9)-O(22)	2.071(4)	O(10)b-O(24)e	2.635(6)	79.5(2)
M(9)-O(24)	2.140(5)	O(22) -O(12)c	3.027(6)	98.3(2)
M(9)-O(24)e	2.144(5)	O(22) -O(17)b	2.629(6)	81.4(2)
Mean	2.035	O(22) -O(24)	2.733(7)	80.9(2)
		O(22) -O(24)e	3.085(7)	94.0(2)
		O(12)c-O(17)b	2.845(6)	94.1(2)
		O(12)c-O(24)e	3.013(8)	95.3(2)
		O(24) -O(17)b	2.873(8)	89.0(2)
		O(24) -O(24)e	2.800(9)	81.6(2)
		Mean	2.864	89.8

M(10) Octahedron

			distance	angle
M(10)- O(3)f	1.954(5)	O(3)f- O(4)g	2.778(7)	91.0(2)
M(10)- O(4)g	1.942(5)	O(3)f- O(6)h	2.821(6)	95.7(2)
M(10)- O(6)h	1.849(5)	O(3)f-O(18)	2.842(8)	87.8(2)
M(10)-O(18)	2.142(5)	O(3)f-O(21)	2.582(6)	81.7(2)
M(10)-O(19)	2.086(5)	O(19) - O(4)g	2.778(6)	87.1(2)
M(10)-O(21)	1.995(4)	O(19) - O(6)h	2.952(8)	97.0(2)
Mean	1.995	O(19) -O(18)	2.704(6)	79.5(2)
		O(19) -O(21)	3.021(7)	95.5(2)
		O(6)h- O(4)g	2.925(7)	100.9(2)
		O(6)h-O(21)	2.953(6)	100.3(2)
		O(18) - O(4)g	2.588(6)	78.5(2)
		O(18) -O(21)	2.679(7)	80.6(2)
		Mean	2.802	89.6

M(11) Octahedron

			distance	angle
M(11)- O(3)f	1.952(4)	O(3)f- O(7)f	2.954(7)	101.2(2)
M(11)- O(7)f	1.869(5)	O(3)f-O(13)h	2.769(7)	89.7(2)
M(11)-O(13)h	1.973(5)	O(3)f-O(20)	2.772(6)	87.4(2)
M(11)-O(20)	2.059(5)	O(3)f-O(21)	2.582(6)	78.3(2)
M(11)-O(21)	2.134(5)	O(22) - O(7)f	2.960(6)	99.7(2)
M(11)-O(22)	2.003(4)	O(22) -O(13)h	2.630(6)	82.8(2)
Mean	1.998	O(72) -O(20)	3.020(7)	96.1(2)
		O(22) -O(21)	2.690(7)	81.1(2)
		O(7)f-O(13)h	2.782(6)	92.7(2)
		O(7)f-O(20)	2.970(8)	98.1(2)
		O(21) -O(13)h	2.891(8)	89.4(2)
		O(21) -O(20)	2.688(6)	79.7(2)
		Mean	2.809	89.7

M(12) Octahedron

			distance	angle
M(12)-O(10)f	1.977(5)	O(10)f-O(13)h	2.801(7)	92.0(2)
M(12)-O(13)h	1.914(5)	O(10)f-O(16)h	2.790(6)	92.9(2)
M(12)-O(16)h	1.870(5)	O(10)f-O(22)	2.807(8)	87.4(2)
M(12)-O(22)	2.085(5)	O(10)f-O(24)	2.635(6)	81.3(2)
M(12)-O(23)	2.034(5)	O(22) -O(13)h	2.733(6)	87.6(2)
M(12)-O(24)	2.068(4)	O(22) -O(16)h	2.996(8)	100.2(2)
Mean	1.991	O(22) -O(22)	2.632(6)	79.4(2)
		O(22) -O(24)	3.034(7)	95.4(2)
		O(16)h-O(13)h	2.930(7)	101.5(2)
		O(16)h-O(24)	2.887(6)	94.2(2)
		O(22) -O(13)h	2.630(6)	82.1(2)
		O(22) -O(24)	2.733(7)	82.3(2)
		Mean	2.800	89.7

A(1) Polyhedron

			distance	angle
A(1)- O(9)h	1.894(5)	O(9)h-O(23)	2.782(6)	95.1(2)
A(1)-O(23)	1.876(4)	O(9)h-O(24)i	2.866(6)	97.1(2)
A(1)-O(24)i	1.929(5)	O(23) -O(24)i	2.825(6)	95.9(2)
Mean	1.900	Mean	2.824	96.0

A(2) Polyhedron

			distance	angle
A(2)- O(2)f	1.859(5)	O(2)f-O(19)	2.855(6)	101.4(2)
A(2)-O(19)	1.831(4)	O(2)f-O(20)j	2.836(6)	100.2(2)
A(2)-O(20)j	1.836(5)	O(19) -O(20)j	2.738(6)	96.6(2)
Mean	1.842	Mean	2.810	99.4

A(3) Polyhedron

			distance	angle
A(3)- O(8)	1.863(5)	O(8)-O(19)	2.932(6)	105.7(2)
A(3)-O(19)	1.815(5)	O(8)-O(20)j	2.919(6)	104.7(2)
A(3)-O(20)j	1.823(5)	O(19)-O(20)j	2.738(6)	97.6(2)
Mean	1.834	Mean	2.863	102.7

a: $\bar{x}, \bar{y}, \bar{z}$;
b: $\bar{x}, 1 - y, -1 - z$;
c: $x, 1 + y, z$;
d: $1 - x, 1 - y, -z$;
e: $1 - x, 2 - y, -1 - z$;
f: $1 + x, 1 + y, z$;
g: $1 - x, \bar{y}, \bar{z}$;
h: $1 + x, y, z$;
i: $1 - x, 1 - y, -1 - z$;
j: $x, y - 1, z$.

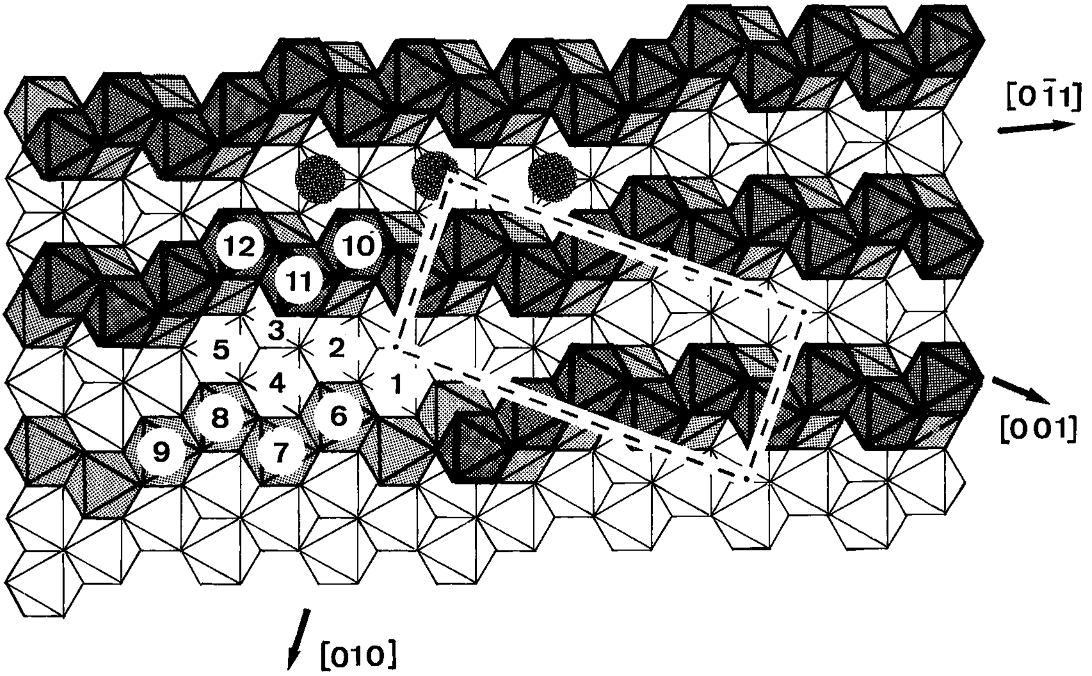

FIG. 3. Polyhedral representation of the structure of hemloite, viewed along a^*. Metal atoms M(1)-M(12) are labeled as in Table 2. A unit cell is outlined. The anion vacancies at the centers of the cuboctahedra, forming one of the 3-member linear clusters, are shown by shaded circles.

between *h*-stacked layers of anions occupy 60% of the octahedral sites and form a V_3O_5-type (Asbrink *et al.* 1959) arrangement of columns of edge-shared octahedra (Fig. 5a). The V_3O_5 structure can be derived formally from the rutile structure by crystallographic shear (CS) on $\{121\}_r$ planes. It represents the first member, $n = 3$, of the homologous series M_nO_{2n-1}. The 3-octahedron-long rutile strings are

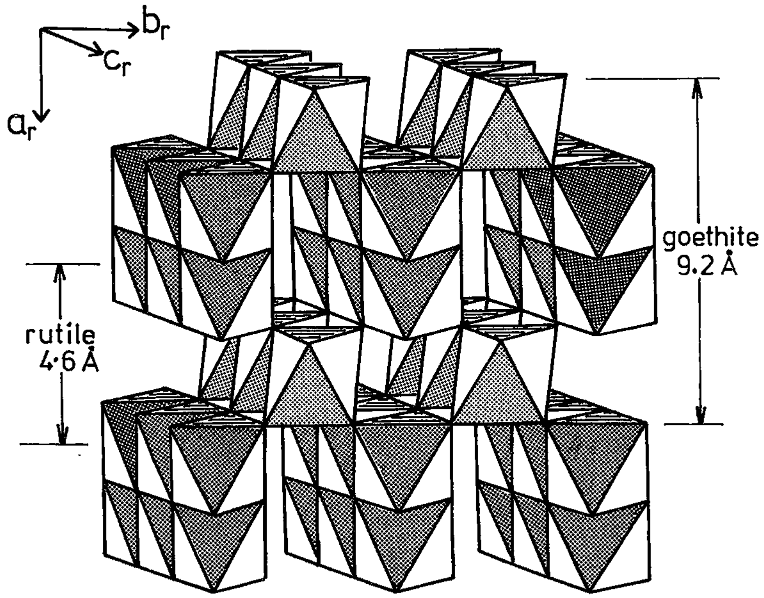

FIG. 4. Polyhedral representation of $(1\ 0\ 0)_r$ intergrowth of rutile and goethite structures. Slabs of this structure alternate with slabs of the tomichite-type structure, parallel to $(0\ 0\ 1)_h$ in hemloite. Subscript r refers to rutile.

evident in Figure 5a. In hemloite, the corresponding layer of metal atoms (Fig. 5b) comprises ordered intergrowths of the $n = 3$ and $n = 4$ homologues. The trace of the $\{121\}_r$ CS plane on this layer is parallel to the intergrowth boundary.

The second type of metal-atom layer in tomichite lies between *c*- and *h*-stacked layers of anions and is illustrated in Figure 5c. Forty percent of the octahedral sites in this layer are occupied, forming α-PbO_2-type zig-zag strings of edge-shared octahedra. Pairs of such metal layers on either side of the *c*-stacked layers of anions are related by a center of symmetry, and the α-PbO_2 chains are fused by edge-sharing into double chains. In the *c*-stacked anionic layers, ordered anionic vacancies occur in strings along $[001]_t$. The anions surrounding these vacancies form cuboctahedra that are joined by edge-sharing into $[001]_t$ chains. In tomichite, an arsenic atom resides within each cuboctahedron, with bonds to the oxygen atoms of a triangular face and with its lone pair of electrons directed toward the center of the cuboctahedron.

The corresponding metal atom and *c*-stacked layer of anions in hemloite are shown in Figure 5d. The α-PbO_2-type strings of the tomichite-like part of the structure are intergrown with 3-octahedron-long linear strings. The fusion of pairs of such strings in adjacent layers by edge-sharing gives short segments of goethite-type structure elements, shown as a polyhedral representation in Figure 4. The tomichite-like sequence of anion vacancies in the *c*-stacked layer is interrupted at the intergrowth boundaries, giving linear clusters of three vacancy-centered anion cuboctahedra. The central vacancy of the cluster is situated at a center of symmetry, (½,0,0).

As AND Sb DISTRIBUTIONS IN HEMLOITE

An important difference between the tomichite-like component of hemloite and tomichite itself lies in the distribution of *A* atoms (As, Sb). In tomichite, one arsenic atom is associated with each anion vacancy, whereas in hemloite, four *A* atoms are associated with only three anion vacancies per unit cell. The distribution of the *A* atoms within a linear cluster of three cuboctahedra is illustrated in Figure 6.

Each cuboctahedron contains two favorable locations for *A* atoms, involving them in pyramidal coordination to triangular faces of an anion, with their lone pairs of electrons directed toward the vacancy. (The remaining six triangular oxygen faces per cuboctahedron would involve the *A* pyramids in face- or multiple edge-sharing with surrounding octahedra.)

The antimony atoms are confined to the terminal cuboctahedra, coordinating to the extreme triangular faces of the cluster. Almost full occupancy of these sites is achieved, with 0.47 Sb + 0.474(4) As.

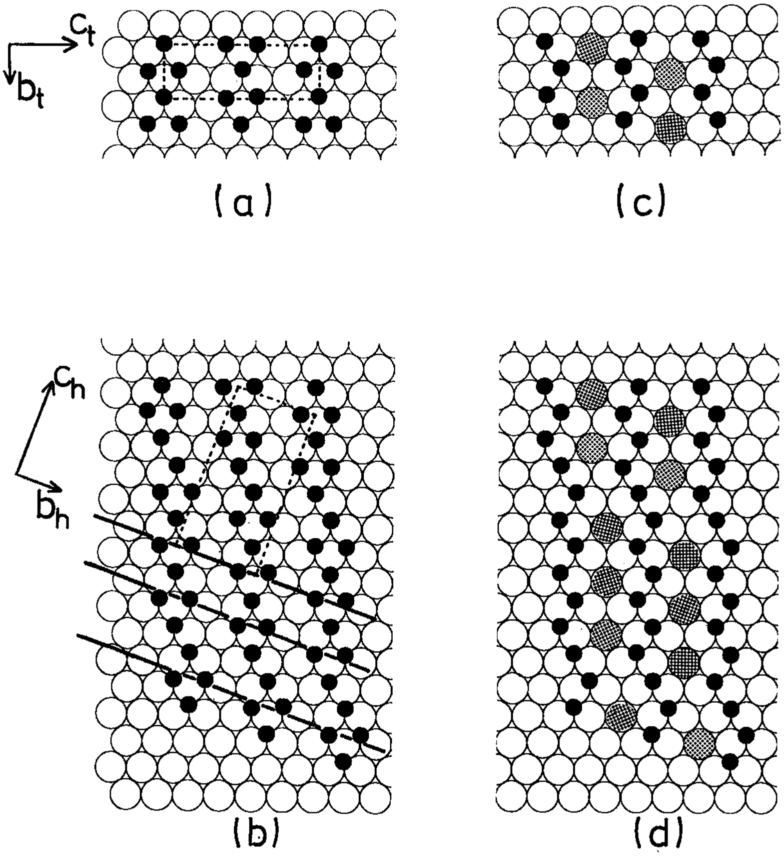

FIG. 5. Equivalent layers of metal atoms in tomichite (a) and (c) and hemloite (b) and (d). Metal atoms between pairs of *h*-stacked layers of anions are shown in (a) and (b), and those between *h*- and *c*-stacked layers of anions are shown in (c) and (d). Small filled circles represent metal atoms, large open circles represent anions, and large shaded circles represent anion vacancies in the *c*-stacked layers of anions. The heavy lines in (b) separate $n=3$ and $n=4$ $\{121\}_r$ rutile CS elements.

The remaining arsenic atoms are distributed over two independent sites, *A*(2) and *A*(3), which coordinate to triangular faces of an anion in adjacent cuboctahedra. The two AO_3 pyramids share a common edge. The sum of the occupancies of these two sites is 1.0, and their short separation, 2.42 Å, requires that they not be occupied simultaneously. The site *A*(2) associated with the central cuboctahedron has an occupancy of 0.685(2), giving 1.37 As atoms in this cuboctahedron. The combined occupancies of *A*(1) and *A*(3) in each of the terminal cuboctahedra is 1.25 (As + Sb). This excess over one *A* atom per cuboctahedron requires that, locally, the cuboctahedra will contain pairs of *A* atoms, coordinated to diagonally opposed triangular faces of an anion. A similar situation occurs in barian tomichite (Grey *et al.* 1987).

The separation of the pairs of *A* atoms is 3.02 Å in each cuboctahedron. The lone pairs of electrons on the opposed *A* atoms are slightly offset from the direct line between the atoms (passing through the center of the cuboctahedron). The calculated values of the angle between the normal to the AO_3 pyramidal base and the line joining the *A* atoms are 9.2, 4.3 and 6.1°, respectively, for *A*(1) to *A*(3).

Within the constraints that (a) the centers of symmetry are maintained locally, (b) simultaneous occupancy of *A*(2) and *A*(3) is not permitted, and (c) the larger Sb atom is limited to sole occupancy of the cuboctahedra, the experimentally determined distribution of *A* atoms distribution can be modeled using a combination of three ordered arrangements. These arrangements are illustrated in Figure 7. The observed distribution corresponds to a statistical mix-

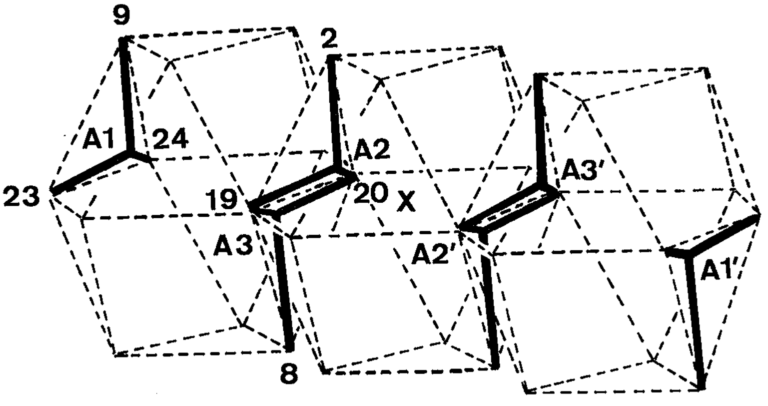

FIG. 6. Linear clusters of three edge-shared cuboctahedra, showing the pyramidal coordination of the three independent *A* atoms. The anions coordinated to *A*(1)-*A*(3) are labeled, consistent with the notation in Table 2. The center of symmetry at (1/2,0,0) is marked with a cross.

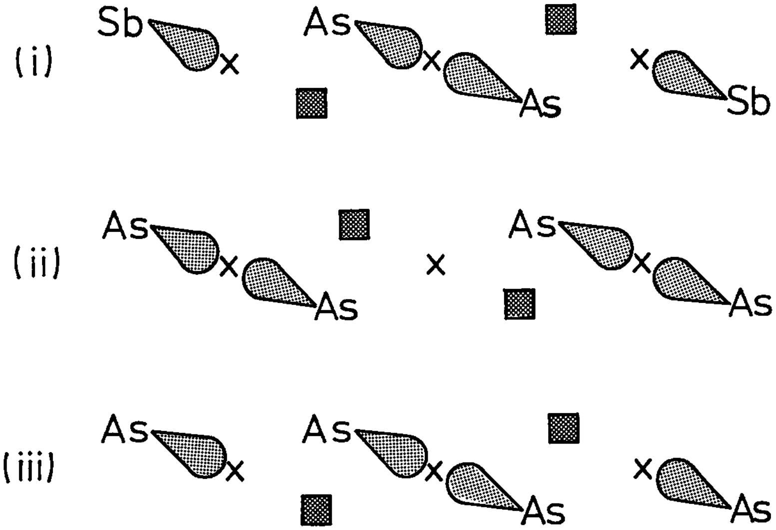

FIG. 7. Three proposed arrangements for local ordering of As and Sb in the linear clusters of 3 cuboctahedra in hemloite. The crosses represent the centers of the cuboctahedra. Lone pairs of electrons are depicted by shaded lobes. Unoccupied pyramidal sites in the cuboctahedra are shown by squares.

ing of 0.47 × (i) + 0.32 × (ii) + 0.21 × (iii).

The average *A*(1)-O distance of 1.900 Å corresponds closely to the calculated value of 1.89 Å for 0.47Sb + 0.47As, using reported average As–O (Hawthorne 1985) and Sb–O (Moore & Araki 1976) distances of 1.78 and 2.01 Å, respectively. For *A*(2) and *A*(3), which always occur with a second *A* atom in the same cuboctahedron, the average *A*–O distances, 1.842 and 1.834 Å, respectively, are considerably longer than the average reported value in a number of recently refined arsenite minerals (Hawthorne 1985).

UNIT-CELL COMPOSITION

The structure refinement for hemloite confirms that the unit cell contains 24 fully occupied *M* sites (octahedral), 48 fully occupied anion sites and close to 4 A sites (As + Sb). Bond-length – bond strength calculations (Table 8; Brown & Altermatt 1985, Trömel 1983) show that the anions O(2) and O(8) are severely undersaturated. A similar situation has been reported for the equivalent anions in derbylite (Moore & Araki 1976) and barian tomichite (Grey *et al.* 1987), and interpreted as occupation of these anion sites by hydroxyl ions. In the case of hemloite, consideration of local ordering of *A*(2) and *A*(3), which are bonded to O(2) and O(8), leads to a calculated value of two hydroxyl groups per unit cell to satisfy local charge-balance requirements. The unit-cell composition was thus normalized to 46 oxygen atoms +2 hydroxyl groups. Using the proportion of cations obtained from the microprobe analysis gives an overall unit-cell composition of $As_{2.98}Sb_{0.94}Ti_{11.25}V_{4.22}Fe_{7.88}Al_{0.65}O_{46}(OH)_2$. In this formula, by analogy with the related minerals derbylite and tomichite, the titanium is considered tetravalent, vanadium is trivalent, and a combination of ferrous and ferric iron is required for charge balance, 1.01 Fe^{2+} + 6.87 Fe^{3+}. The presence of some iron in the divalent state is indicated by valence-sum calculations (Table 8), which give valence summations less than three at sites *M*(1), *M*(4) and *M*(9). Ferrous iron has been confirmed in a sample of derbylite (Mellini *et al.* 1983). The proposed combination of Fe^{2+}, Fe^{3+} and V^{3+} is consistent with known valence states of these elements (from Mössbauer and magnetic measurements) where they occur together in octahedral sites in Fe_2VO_4–FeV_2O_4 (Wakihara *et al.* 1971) and (Fe, V)$_2$O$_3$ (Shirane *et al.* 1962).

No attempt was made to refine individual distributions of cations in the sites *M*(1)-*M*(12) because of the number of cations involved and the small differences in their scattering power. However, a consideration of the refined thermal parameters (Table 5), the heights of atomic peaks in Fourier maps, and results of valence-sum calculations (Table 8), lead to some general observations. Iron atoms are the dominant contributors to sites *M*(1), *M*(3), *M*(4) and *M*(9), and titanium atoms are dominant in the smallest site *M*(2). Aluminum is probably also concentrated in the smallest site *M*(2). The remaining titanium and vanadium atoms appear to be relatively uniformly distributed over the remaining seven *M* sites.

TABLE 8. VALENCE SUMS FOR CATIONS AND ANIONS IN HEMLOITE

(a) Cations[1]

Cation	Valence Sum	Cation	Valence Sum	Cation	Valence Sum
A(1)	2.88	M(3)	3.07	M(8)	3.65
A(2)	2.61	M(4)	2.87	M(9)	2.91
A(3)	2.69	M(5)	3.50	M(10)	3.57
M(1)	2.84	M(6)	3.62	M(11)	3.47
M(2)	3.60	M(7)	3.45	M(12)	3.54

(b) Anions

Anion	Valence Sum	Anion	Valence Sum	Anion	Valence Sum
O(1)	1.95	O(9)	2.04	O(19)[3]	1.79
O(2)[2]	2.08	O(10)	1.89		1.82
	1.24	O(11)	1.91	O(20)[3]	1.78
O(3)	1.91	O(12)	1.87		1.82
O(4)	1.92	O(13)	1.96	O(21)	1.86
O(5)	1.92	O(14)	1.93	O(22)	1.83
O(6)	1.92	O(15)	1.86	O(23)	2.06
O(7)	1.92	O(16)	2.03	O(24)	2.05
O(8)[2]	2.11	O(17)	1.98		
	1.27	O(18)	1.87		

1. Bond-valence parameters for As^{3+} and Sb^{3+} were taken from Brown & Altermatt (1985) and for Ti, V and Fe from Trömel (1983). Cations (M1), M(3), M(4) and M(9) were treated as Fe only sites with remaining M-type cations as mixed Ti-V sites. 2. The two values listed correspond to the associated A-type site being occupied or vacant respectively; see text and Figure 6. 3. The two values correspond to A(2) and A(3) respectively, completing the coordination environment of the oxygen atom; see text and Figure 6.

ACKNOWLEDGEMENTS

We thank the University of Melbourne for the award of a Special Studies Programme to B.F.H. and for the use of the Enraf-Nonius CAD4 Diffractometer located in its Department of Inorganic Chemistry. We thank A.C. Roberts, Geological Survey of Canada, for assistance in obtaining an X-ray powder pattern of the mineral. Comments on an earlier version of this manuscript by J. Chisholm, British Museum (NH), are most appreciated.

REFERENCES

ASBRINK, S., FRIBERG, S., MAGNELI, A. & ANDERSSON, G. (1959): Note on the crystal structure of trivanadium pentoxide. *Acta Chem. Scand.* **13**, 603.

BROWN, I.D. & ALTERMATT, D. (1985): Bond-valence parameters obtained from a systematic analysis of the inorganic crystal structure database. *Acta Crystallogr.* **B41**, 244-247.

CRIDDLE, A.J., STANLEY, C.J., CHISHOLM, J.E. & FEJER, E.E. (1983): Henryite, a new copper–silver telluride from Bisbee, Arizona. *Bull. Minéral.* **106**, 511-517.

DE WOLFF, P.M. (1959): Interpretations of some γ-MnO$_2$ diffraction patterns. *Acta Crystallogr.* **12**, 341-345.

EMBREY, P.G. & CRIDDLE, A.J. (1978): Error problems in the two-media method of deriving the optical constants *n* and *k* from measured reflectances. *Am. Mineral.* **63**, 853-862.

GALOPIN, R. & HENRY, N.F.M. (1972): *Microscopic Study of Opaque Minerals.* McCrone Research Associates, London.

GREY, I.E., MADSEN, I.C. & HARRIS, D.C. (1987): Barian tomichite, $Ba_{0.5}(As_2)_{0.5}Ti_2(V,Fe)_5O_{13}(OH)$, its crystal structure and relationship to derbylite and tomichite. *Am. Mineral.* **72**, 201-208.

HARRIS, D.C. (1986a): The minerals in the main Hemlo gold deposit, Ontario. *Geol. Surv. Can., Pap.* **86-1A**, 49-54.

______ (1986b): Mineralogy and geochemistry of the main Hemlo gold deposit, Hemlo, Ontario, Canada. *In* Proc. Gold '86, an International Symposium on the Geology of Gold: (Toronto, 1986; A.J. Macdonald, ed.), 297-310.

HAWTHORNE, F.C. (1985): Schneiderhohnite, $Fe^{2+}Fe_3^{3+}As_5^{3+}O_{13}$, a densely packed arsenite structure. *Can. Mineral.* **23**, 675-679.

INTERNATIONAL TABLES FOR X-RAY CRYSTALLOGRAPHY (1974) Vol. IV. Kynoch Press, Birmingham, England.

MAIN, P., WOOLFSON, M.M. & GERMAIN, L. (1977): *MULTAN: A Computer Programme for the Automatic Solution of Crystal Structures.* University of York Printing Unit, York, England.

MANDARINO, J.A. (1979): The Gladstone–Dale relationship. III. Some general applications. *Can. Mineral.* **17**, 71-76.

______ (1981): The Gladstone–Dale relationship. IV. The compatibility concept and its application. *Can. Mineral.* **19**, 441-450.

MELLINI, M., ORLANDI, P. & PERCHIAZZI, N. (1983): Derbylite from Buca della Vena mine, Apuan Alps, Italy. *Can. Mineral.* **21**, 513-516.

MOORE, P.B. & ARAKI, T. (1976): Derbylite, $Fe^{3+}{}_4\ Ti^{4+}{}_3\ Sb^{3+} + O_{13}(OH)$, a novel close-packed oxide structure. *Neues Jahrb. Mineral., Abh.* **126**, 292-303.

SHELDRICK, G.M. (1976): SHELX-76: *A Programme for Crystal Structure Determination.* University of Cambridge, Cambridge, England.

SHIRANE, G., COX, D.E. & RUBY, S.L. (1962): Mössbauer study of isomer shift, quadrupole interaction, and hyperfine field in several oxides containing Fe(57). *Phys. Rev.* **125**, 1158-1165.

TRÖMEL, M. (1983): Empirische Beziehungen zu den Bindungslängen in Oxiden. 1. Die Nebengruppenelemente Titan bis Eisen. *Acta Crystallogr.* **B39**, 664-669.

WAKIHARA, M., SHIMIZU, Y. & KATSURA, T. (1971): Preparation and magnetic properties of the FeV_2O_4–Fe_3O_4 system. *J. Solid State Chem.* **3**, 478-483.

Received July 18, 1988, revised manuscript accepted January 4, 1989.